HHS Public Access

Author manuscript

Angew Chem Int Ed Engl. Author manuscript; available in PMC 2017 December 23.

Published in final edited form as:

Angew Chem Int Ed Engl. 2016 December 23; 55(52): 16039–16043. doi:10.1002/anie.201609043.

Tailoring Renal Clearance and Tumor Targeting of Ultrasmall Metal Nanoparticles with Particle Density

Shaoheng Tang, **Chuanqi Peng**, **Jing Xu**, **Bujie Du**, **Qingxiao Wang**, **Rodrigo D. Vinluan III**, **Mengxiao Yu**, **Moon J. Kim**, and **Jie Zheng**[*]

Department of Chemistry, The University of Texas at Dallas, 800 W. Campbell Rd., Richardson, TX, 75080, USA

Department of Materials Science and Engineering, The University of Texas at Dallas, USA

Abstract

Identifying key factors that govern in vivo behaviors of nanomaterials is critical to future clinical translation of nanomedicines. Shadowed by size-, shape- and surface-chemistry effects, the impact of particle core density on clearance and tumor targeting of inorganic nanoparticles (NPs) remains largely unknown. By utilizing a class of ultrasmall metal NPs with the same size and surface chemistry but different densities as model, we found that both renal clearance and passive tumor targeting of the NPs are strongly correlated with their densities: with the decrease of particle density, renal-clearance efficiency exponentially increased in the early elimination phase but passive tumor targeting was linearly decreased. Through systematic investigation on their pharmacokinetics, biodistribution and kidney filtration, we found that lower density NPs more easily distribute in the body and have shorter retention in highly permeable organs such as kidneys than the higher ones. These density-dependent in vivo behaviors are likely due to the fact that high-density AuNPs marginated to the blood vessel walls more quickly than low-density NPs; as a result, they circulated slowly in the laminar blood flow than the low-density ones. These new findings highlight the importance of particle density in tailoring of in vivo behaviors of engineering NPs and might open up a new pathway for designing nanomedicines with desired functionalities together with other key factors.

Unraveling key factors that are involved in nano-bio interactions *in vivo* is fundamental importance of translating nanomedicines into the clinics.[1] In the past decades, size, shape and surface chemistry of inorganic NPs have found to significantly affect their *in vivo* behaviors.[2] For example, Chan et al. found that gold nanoparticles (AuNPs) with different sizes show distinct tumor uptakes and penetration depths.[3] Among the AuNPs with sizes ranging from 20 to 100 nm, the small 20 nm AuNPs exhibited the lower accumulation but larger penetration depth in the tumor than others. Xia et al. investigated shape-effect on *in vivo* behaviors of gold nanostructures and found that nanospheres have longer blood circulation and higher tumor uptake over other shaped Au nanostructures.[4] Moreover, various surface chemistries have been widely used to manipulate *in vivo* behaviors of nanomedicines.[5]

[*] jiezheng@utdallas.edu.

While our fundamental understanding of nano-bio interaction of inorganic NPs *in vivo* have been greatly advanced in the past decades, core density, another intrinsic material characteristics of inorganic NPs, has not attracted enough attention and only very limited studies on density effect on nano-bio interactions have been done.[6] For instance, Toy et al. found that ~60 nm polymeric NPs can marginate much further than the same sized iron oxide or gold NPs in microfluidic channels even though they have the same diffusion coefficient and the gravitational force is negligible for these sized NPs.[6c] This experimental result is also consistent with the theoretical modeling on margination of nanoparticles to blood vessel wall, where relative density difference between NPs and blood plays a significant role in margination time of 50nm particles: high density NPs tends to have short margination time, more quickly reach endothelium and have strong interactions with blood vessel walls.[6a] As a result, the light NPs and can circulate in the body much faster than the heavy NPs.[6a]

On an even smaller size scale, however, whether density can still significantly affect *in vivo* behaviors of inorganic NPs with different compositions is not clear even though they exhibited distinct clearance efficiency and tumor targeting.[7] For instance, Choi et al. systematically investigated renal clearance of cysteine coated CdSe/ZnS quantum dots (QDs) and found that almost all the 4.36 nm QDs can be renally cleared within 24 h after intravenous injection.[8] Similar to these QDs, silica NPs also exhibited very high renal clearance efficiencies: about 70 percent of injected dose (%ID) of silica NPs was excreted in urine at 24 h post injection (p.i.).[9] However, the clearance of glutathione (GS)-coated AuNPs through urinary system was relatively slow, where less than 50 %ID of GS-AuNPs were cleared out of the body into the urine at 24 h p.i. but they exhibited much longer blood retention and higher passive tumor targeting than those of silica dots and QDs.[10] Not limited to these three types of renal clearable NPs, other renal clearable inorganic NPs with different compositions also exhibit distinct renal clearance and tumor targeting.[11] However, shadowed by differences in size and surface chemistry among these ultrasmall NPs, it is highly challenging to unravel density effect on *in vivo* behaviors of ultrasmall NPs.

Herein, we present a quantitative study of the density effect on renal clearance and tumor targeting of ultrasmall metal NPs by synthesizing a class of glutathione-coated noble metal NPs with the same size and surface chemistry but different densities, including glutathione coated AuNPs (GS-AuNPs), AgNPs (GS-AgNPs) and two kinds of Au-Ag alloyed NPs (GS-Au/Ag(1)NPs and GS-Au/Ag(2)NPs). By quantifying their *in vivo* behaviors (renal clearance efficiencies, pharmacokinetics, kidney filtration, biodistribution and tumor targeting), we found that as the NPs' core density increased, their renal clearance efficiencies in the early elimination stage (2 h p.i.) exponentially decreased but their passive tumor targeting efficiencies linearly increased. Quantitative analysis of their pharmacokinetics parameters showed that origin of density-dependent renal clearance and targeting is intrinsically because the NPs with lower density are more easily distributed in the body and filtrated through the kidneys, which was further supported by noninvasive fluorescence imaging of kidney clearance of the GS-AuNPs and GS-AgNPs. These fundamental understandings clearly indicated that particle density could serve as another key factor to tailor *in vivo* behaviors of inorganic NPs for different biomedical applications.

Four types of ultrasmall noble metal NPs were synthesized in a way that they have the same antifouling surface coating, glutathione and identical size. GS-AuNPs and GS-AgNPs were prepared according to our previously described thermal reduction method.[12] Briefly, the precursor solutions were prepared by dissolving the glutathione and $HAuCl_4$ (molar ratio of 1:0.8) or $AgNO_3$ (molar ratio of 3.4:1) in 40 *ml* water and then the mixture was heated at 95 °C for 0.5 h and 37 h, respectively. After purification, ~2.6 nm NIR-emitting GS-AuNPs and GS-AgNPs with ~3.1 nm hydrodynamic diameter (HD) were obtained (Figure S1). Little change in UV-Vis absorption of GS-AgNPs after being incubated with phosphate buffer saline (PBS) containing 10% fetal bovine serum (FBS) at 37 °C for 72 h indicate that GS-AgNPs were fairly stable in physiological environment (Figure S2). To create more metal NPs with the same size and surface coating but different core densities, we also synthesized Au-Ag alloy NPs through co-reduction method. Briefly, $HAuCl_4$ and $AgNO_3$ solution were mixed at molar ratios of 1:1.3 and 1:1, respectively, followed by chemical reduction with freshly prepared $NaBH_4$ solution (0.5M) in the presence of GS in 4 *ml* distilled water at room temperature. After purification, glutathione coated Au-Ag NPs (GS-Au/AgNPs) with ~3.1 nm HD were obtained. (Figure 1 A,B). Scanning transmission electron microscopy (STEM) imaging coupled with energy-dispersive X-ray spectroscopy (EDS) further confirmed the successful synthesis of the alloyed GS-Au/AgNPs. As shown in Figure 1C, elemental-mapping analysis indicates that all the Au and Ag atoms are homogeneously mixed within a single nanostructure. The accurate Au/Ag atomic ratios of them were determined using inductively coupled plasma mass spectrometry (ICP-MS), which were 1:8.4 and 1:0.64, corresponding to 11.4 g/cm^3 and 15.9 g/cm^3 for GS-Au/Ag(1)NPs and GS-Au/Ag(2)NPs, respectively. Together with GS-AuNPs (19.3 g/cm^3) and GS-AgNPs (10.5 g/cm^3), these ultrasmall metal NPs with the same size and surface chemistry can serve as model to quantitatively unravel how the core density affects renal clearance and tumor targeting of ultrasmall metal NPs.

Antifouling nature of glutathione renders these ultrasmall metal NPs high resistance to serum protein adsorption and allows us to unravel density effect without interference from serum protein in the physiological environment (Figure S3). Four groups of BALB/c mice (n=3) were intravenously injected with the four types of ultrasmall metal NPs respectively, and urine samples were collected at various time points and then analyzed with ICP-MS (Please see SI for the detailed procedure). As shown in Figure 2A, those ultrasmall metal NPs exhibited comparable renal clearance efficiencies at 48 h p.i., 51.36 %ID, 52.99 %ID, 48.69 %ID and 45.57 %ID, for GS-AgNPs, GS-Au/Ag(1)NPs, GS-Au/Ag(2)NPs and GS-AuNPs, respectively. However, their renal clearance kinetics is significantly different and strongly density-dependent: the NPs with lower density are more efficiently excreted into urine in the early clearance stage. At 2 h p.i. the highest renal clearance was observed from the GS-AgNPs (45.87%ID), followed by GS-Au/Ag(1)NPs (36.90%ID), GS-Au/Ag(2)NPs (31.22%ID) and GS-AuNPs (29.19%ID). Combined with our previous results, where GS-CuNPs (8.9g/cm^3) with 2.7nm HD exhibited even higher clearance efficiency (~ 60 %ID, at 2 h. p.i.),[13] we found that the amount of NPs excreted into urine at 2 h p.i. is exponentially decreased with the increase of the particle density (Figure 2B).

Strong density-dependent renal clearance is consistent with our pharmacokinetics studies of these metal NPs. Although all the metal NPs exhibit two-compartment pharmacokinetics

with very short distribution half-lives and relatively long elimination half-lives, several key parameters including distribution half-life ($T_{1/2\alpha}$), elimination half-life ($T_{1/2\beta}$), volume of distribution (V_d), clearance (*CL*) and area under the curve (AUC), derived from their pharmacokinetics, are significantly different among these four different types of metal NPs (Figure 2 C and Table S1). It is well known that the parameter V_d reflects the degree of how a foreign material is distributed in organs and tissues and the *CL* reflects organism's capability of removing a given material via excretion or metabolism.[14] As shown in Figure 2 D,E, with the decrease of particle density from 19.3 g/cm^3 (GS-AuNPs) to 10.5 g/cm^3 (GS-AgNPs), both V_d and *CL* were increased from 2.98 ml and 0.54 ml h^{-1} to 8.97 ml and 2.25 ml h^{-1}, respectively, following a exponentially increase with the particle density. These results indicate that reducing particle density not only can greatly expedite the distribution of NPs in the body but also can enhance the renal clearance of NPs out of the body. Moreover, because of the differences in the renal clearance, the blood retention, characterized as area under the curves (AUCs), of these different density metal NPs is also distinct, following exponentially increase with the increase of particle density (Figure 2 F). Since passive tumor targeting is mainly governed by AUCs of NPs in the blood,[3, 15] GS-AuNPs exhibited the highest tumor targeting and the targeting efficiency of these metal NPs was found to linearly depend on the particle density (Figure 2 G).

To further unravel the detailed excretion mechanism, we took advantage of strong intrinsic near infrared (NIR) fluorescence of GS-AuNPs and GS-AgNPs (Figure S4) and noninvasively monitored the fluorescence signals from kidneys and background tissues of BALB /c mice (n=3) after injected with GS-AuNPs and GS-AgNPs, respectively (Movie S1 and Movie S2), which show distinct distribution and clearance kinetics. The normalized time fluorescence intensity curves (NTFICs) of kidneys were obtained through the whole-body imaging (Figure 3 A,B) and two key parameters of the NTFICs, time to reach the maximum fluorescence intensity (TMFI) and clearance rate (defined as the decline percentage at 60 min=[(peak value-intensity at 60 min p.i.) / peak value] × 100%), were extracted and compared (Figure S5). For GS-AuNPs, the average fluorescence intensity of the kidney region rapidly increased to the maximum value at about 2 min p.i., followed by a rapid decrease. At 1 h p.i., kidney fluorescence signal was dropped about ~80% of TMFI (Figure 3 C). On the other hand, it took 11.83±1.75 min for the fluorescence signal of kidneys of the mice injected with GS-AgNPs to reach its maximum. In addition, unlike the kidney signal from the mice injected with GS-AuNPs, the kidney signal of the mice injected with GS-AgNPs maintained a constant intensity with a negligible decrease (1.43%) even though much more GS-AgNPs were eliminated into the bladder than GS-AuNPs in the early elimination phase. In addition, the clearance of GS-AgNPs from background tissues was also slower than that of GS-AuNPs (Figure 3 D and S6). Combining with V_d values, the accumulation and clearance kinetics of these two different density NPs indicated that low-density GS-AgNPs more easily distributed in the body through the blood flow and accumulated in the both kidney and background tissues. Indeed, more detailed fluorescence imaging of the distributions of GS-AgNPs and GS-AuNPs in the kidneys at an early injection time point (7 min. p.i.) also confirm that low-density GS-AgNPs not only accumulated in the cortex region like GS-AuNPs (Figure 3 E) but also penetrated into the

medulla regions (Figure 3F), especially the region near the renal pelvis much more than GS-AuNPs (Figure 3G).

To gain more insight in *in vivo* clearance of these ultrasmall metal NPs, we quantified their 7-min and 48-h biodistribution and compared the differences in the biodistributions between these time points. As shown in Figure 4A and S7, at 7 min. p.i., these metal NPs mainly accumulated in the highly permeable organs - kidney, liver and intestine; however, the accumulation of GS-AgNPs in these organs is much higher than GS-AuNPs, suggesting that low-density GS-AgNPs reached the kidney more quickly than high-density GS-AuNPs; as a result, more GS-AgNPs were eliminated through the urinary system. In addition, head-to-head comparison on their biodistributions at 48 h p.i. shows that the percentages of the decreases in these organs are quite different between GS-AuNPs and GS-AgNPs (Figure S8). As shown in Figure 4B, 6.7±2.4, 2.6±0.6 and 2.4±1.6 %ID/g more of the GS-AgNPs were cleared out from the kidney, liver and intestine than GS-AuNPs, further suggesting that low-density AgNPs have lower affinity to blood vessels and shorter retention time in the highly vascular organs and than high-density AuNPs. These results are consistent with the previous theoretical modelling that lower-density ~50nm NPs tend to circulate in the blood vessel much faster than the higher ones because of their long margination time[6]. Based on these experimental results and previous studies on margination of large NPs (>50nm) and blood vessels or microfluidic channels,[6] we hypothesize that even at a smaller size scale (~3nm), such density-dependent margination observed at an size scale >50nm still valid. As shown in Figure 4C, because the densities of AgNPs and AuNPs are much larger than that of blood, both of them marginate in the blood flow. Since gold density is nearly two times larger than silver, GS-AuNPs marginate to the blood vessel walls faster than GS-AgNPs; as a result, in laminar blood flow, GS-AgNPs circulate faster than GS-AuNPs, resulting in more rapid kidney clearance and short blood retention and lower tumor targeting.

In summary, using a class of ultrasmall metal NPs with the same sizes and surface chemistry but different densities as model, we systematically investigated density-effect on renal clearance, kidney filtration, pharmacokinetics and tumor targeting of these metal NPs. Our results show that renal clearance is exponentially decreased in the early elimination phase with the increase of particle density and tumor targeting is linearly dependent on particle density. Such density-dependent in vivo behaviors of ultrasmall metal NPs very likely originate from density-dependent margination, where high-density gold nanoparticles more quickly marginate to the blood wall; as a result, in the laminar blood flow, GS-AuNPs circulated slowly than GS-AgNPs in the blood vessel, leading to slower renal clearance, longer blood retention as well as higher tumor targeting than GS-AgNPs. This observation is consistent with the previous theoretical modeling and experimental measurement of margination and flow of large NPs (>50nm), suggesting that density effect on *in vivo* behaviors that were observed at large size scale might be still valid even at few-nm size scale as long as the particle density is much larger than blood density. Our future work is to continue understanding margination of these ultrasmall metal NPs in the blood vessels. Nevertheless, these quantitative and fundamental understandings of particle-density effect on *in vivo* behaviors of the NPs offer a new but generalizable strategy, in addition to size, shape and surface chemistry effects, for precisely controlling clearance and targeting nanomedicines in their future translation to the clinics.

Supplementary Material

Refer to Web version on PubMed Central for supplementary material.

Acknowledgments

[b] This work was supported by the NIH R01DK103363, CPRIT (RP120588, RP140544), Louis Beecherl, Jr. endowment funds and the start-up fund from The University of Texas at Dallas (J.Z.).

REFERENCES

[1]. Wilhelm S, Tavares AJ, Dai Q, Ohta S, Audet J, Dvorak HF, Chan WCW. Nat Rev Mater. 2016; 5:16014–16026.

[2]. a) Zhang YN, Poon W, Tavares AJ, McGilvray ID, Chan WCW. J Control Release. 2016; 1:1–17.b) Chithrani BD, Ghazani AA, Chan WCW. Nano Lett. 2006; 6:662–668. [PubMed: 16608261] c) Chou LYT, Chan WCW. Adv Healthc Mater. 2012; 1:714–721. [PubMed: 23184822] d) Kim BH, Hackett MJ, Park J, Hyeon T. Chem Mate. 2014; 26:59–71.e) Sykes EA, Chen J, Zheng G, Chan WCW. ACS Nano. 2014; 8:5696–5706. [PubMed: 24821383] f) Lazarovits J, Chen YY, Sykes EA, Chan WCW. Chem Commun. 2015; 51:2756–2767.g) Huynh E, Rajora MA, Zheng G. Wiley Interdiscip Rev Nanomed Nanobiotechnol. 2016 doi: 10.1002/wnan.1398.

[3]. Perrault SD, Walkey C, Jennings T, Fischer HC, Chan WCW. Nano Lett. 2009; 9:1909–1915. [PubMed: 19344179]

[4]. Black KCL, Wang Y, Luehmann HP, Cai X, Xing W, Pang B, Zhao Y, Cutler CS, Wang LV, Liu Y, Xia Y. ACS Nano. 2014; 8:4385–4394. [PubMed: 24766522]

[5]. a) Mo R, Jiang T, Gu Z. Angew Chem Int Ed Engl. 2014; 53:5815–5820. [PubMed: 24764317] b) Lu Y, Hu Q, Lin Y, Pacardo DB, Wang C, Sun W, Ligler FS, Dickey MD, Gu Z. Nat Commun. 2015; 6c) Sun W, Ji W, Hall JM, Hu Q, Wang C, Beisel CL, Gu Z. Angew Chem Int Ed Engl. 2015; 54:12029–12033. [PubMed: 26310292] d) Yu J, Zhang Y, Ye Y, DiSanto R, Sun W, Ranson D, Ligler FS, Buse JB, Gu Z. Proc. Natl. Acad. Sci. U.S.A. 2015; 112:8260–8265. [PubMed: 26100900]

[6]. a) Decuzzi P, Lee S, Bhushan B, Ferrari M. Ann Biomed Eng. 2005; 33:179–190. [PubMed: 15771271] b) Toy R, Hayden E, Shoup C, Baskaran H, Karathanasis E. Nanotechnology. 2011; 22:115101–115101. [PubMed: 21387846] c) Thompson AJ, Eniola-Adefeso O. Acta Biomater. 2015; 21:99–108. [PubMed: 25870170]

[7]. a) Choi HS, Ipe BI, Misra P, Lee JH, Bawendi MG, Frangioni JV. Nano Lett. 2009; 9:2354–2359. [PubMed: 19422261] b) Huang X, Zhang F, Zhu L, Choi KY, Guo N, Guo J, Tackett K, Anilkumar P, Liu G, Quan Q, Choi HS, Niu G, Sun Y-P, Lee S, Chen X. ACS Nano. 2013; 7:5684–5693. [PubMed: 23731122] c) Choi HS, Liu W, Misra P, Tanaka E, Zimmer JP, Itty Ipe B, Bawendi MG, Frangioni JV. Nat Biotech. 2007; 25:1165–1170.d) Yang Y, Liu J, Liang C, Feng L, Fu T, Dong Z, Chao Y, Li Y, Lu G, Chen M, Liu Z. ACS Nano. 2016; 10:2774–2781. [PubMed: 26799993] e) Zhou M, Li J, Liang S, Sood AK, Liang D, Li C. ACS Nano. 2015; 9:7085–7096. [PubMed: 26098195]

[8]. Choi HS, Liu W, Liu F, Nasr K, Misra P, Bawendi MG, Frangioni JV. Nat Nano. 2010; 5:42–47.

[9]. Burns AA, Vider J, Ow H, Herz E, Penate-Medina O, Baumgart M, Larson SM, Wiesner U, Bradbury M. Nano Lett. 2009; 9:442–448. [PubMed: 19099455]

[10]. a) Liu J, Yu M, Ning X, Zhou C, Yang S, Zheng J. Angew Chem Int Ed Engl. 2013; 52:12572–12576. [PubMed: 24123783] b) Zhou C, Long M, Qin Y, Sun X, Zheng J. Angew Chem Int Ed Engl. 2011; 50:3168–3172. [PubMed: 21374769] c) Yu M, Liu J, Ning X, Zheng J. Angew Chem Int Ed Engl. 2015; 54:15434–15438. [PubMed: 26510715] d) Liu J, Duchesne PN, Yu M, Jiang X, Ning X, Vinluan RD, Zhang P, Zheng J. Angew Chem Int Ed Engl. 2016; 55:8894–8898. [PubMed: 27348584] e) Sun S, Ning X, Zhang G, Wang Y-C, Peng C, Zheng J. Angew Chem Int Ed Engl. 2016; 7:2421–2424.f) Yu M, Zhou J, Du B, Ning X, Authement C, Gandee L, Kapur P, Hsieh J-T, Zheng J. Angew Chem Int Ed Engl. 2016; 8:2787–2791.

[11]. a) Chen H, Wang GD, Tang W, Todd T, Zhen Z, Tsang C, Hekmatyar K, Cowger T, Hubbard RB, Zhang W, Stickney J, Shen B, Xie J. Adv Mater. 2014; 26:6761–6766. [PubMed: 25178894] b) Tang S, Chen M, Zheng N. Small. 2014; 10:3139–3144. [PubMed: 24729448]

[12]. Zhou C, Hao G, Thomas P, Liu J, Yu M, Sun S, Öz OK, Sun X, Zheng J. Angew Chem Int Ed Engl. 2012; 51:1011–10122.

[13]. Yang S, Sun S, Zhou C, Hao G, Liu J, Ramezani S, Yu M, Sun X, Zheng J. Bioconjug Chem. 2015; 26:511–519. [PubMed: 25674666]

[14]. Greenblatt DJ. Annu Rev Med. 1985; 36:421–427. [PubMed: 3994325]

[15]. Li S-D, Huang L. Mol Pharmaceut. 2008; 5:496–504.

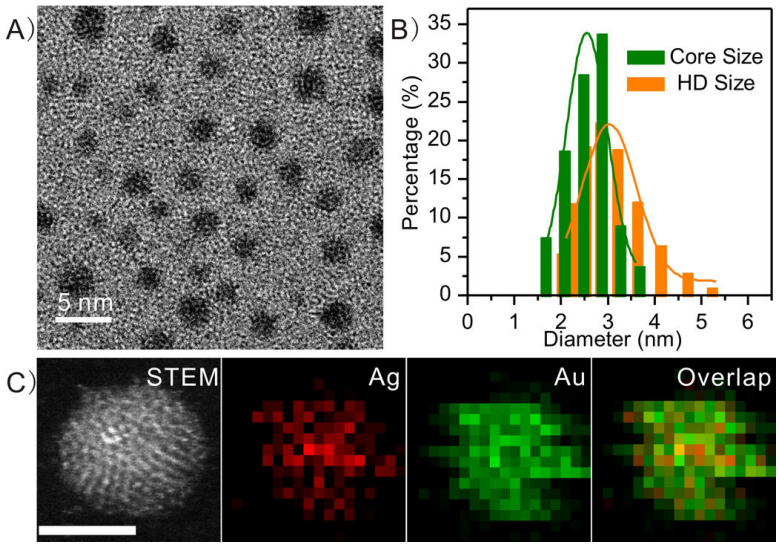

Figure 1.

Characterization of glutathione-coated Au-Ag alloy nanoparticles (GS-Au/AgNPs). A) Typical transmission electron microscopy (TEM) image of GS-Au/AgNPs. B) A core size of 2.6±0.2 nm, and dynamic light scattering analysis showing a hydrodynamic diameter (HD) of 3.1±0.3 nm in aqueous solution. C) STEM and EOS mapping images of the GS-Au/AgNPs with a Au/Ag molar ratio of 1.4. scale bar=2 nm

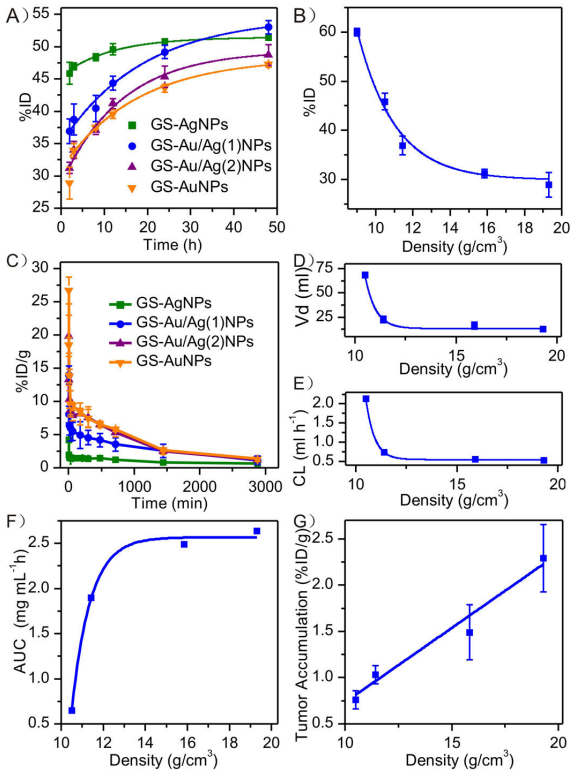

Figure 2.

In vivo behaviors of ultrasmall glutathione coated metal nanoparticles. A) Renal clearance of four kinds of metal NPs within 48 h p.i.. B) The exponential relationship between 2-h renal clearance (RC) and particle core density (d), expressed as: $RC=2.5*10^3\exp(-d/2.1)+29.9$ $R^2=0.98$ C) Pharmacokinetics of the NPs. The pharmacokinetic parameters were determined by fitting the data with a two-compartment model. D–F) The relationships between the density and the three main pharmacokinetic parameters: volume of distribution (V_d and the relationship can be expressed as: $V_d=4.31*\exp(-d/0.51)+13.3$ $R^2=0.99$ (D), clearance (*CL*) and the relationship can be expressed as follow: $CL=6.55*\exp(-d/0.43)+0.55$ $R^2=0.99$ (E) and area under the curve (AUC) and the relationship can be expressed as: $AUC=2.7*10^5\exp(-d/0.88)+2.5$, $R^2=0.99$ (F), were calculated. G) The relationship between tumor accumulation (TA) and density which can be expressed as: $TA=0.16d-0.87$, $R^2=0.99$.

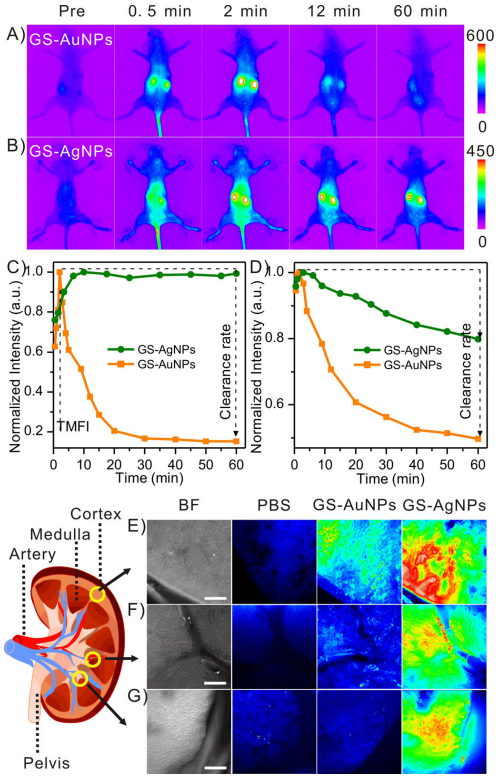

Figure 3.

Fluorescence imaging of renal clearance of GS-AuNPs and GS-AgNPs. A,B) Representative whole-body noninvasive fluorescence images of mice injected with the GS-AuNPs (A) and the GS-AgNPs (B) (Ex/Em filters: 710/830 nm). C,D) Representative time-fluorescence intensity curves (TFICs) of kidneys (C) and background (D) in the two groups of BALB/c mice (n=3) intravenously injected with GS-AuNPs and GS-AgNPs, respectively. Two parameters were extracted from the kidney TFICs: time to achieve maximum fluorescence intensity (TMFI) and clearance rate (defined as the clearance percentage at 60 min=[(peak value-intensity at 60 min) / peak value] × 100%). E–G) Kidney penetration study. Bright field (BF) and Fluorescence images of kidney slices after iv injection of PBS, GS-AuNPs and GS-AgNPs. Three representative regions were selected: cortex (E), medulla regions near the artery (F) and pelvis (G). scale bar=200 μm.

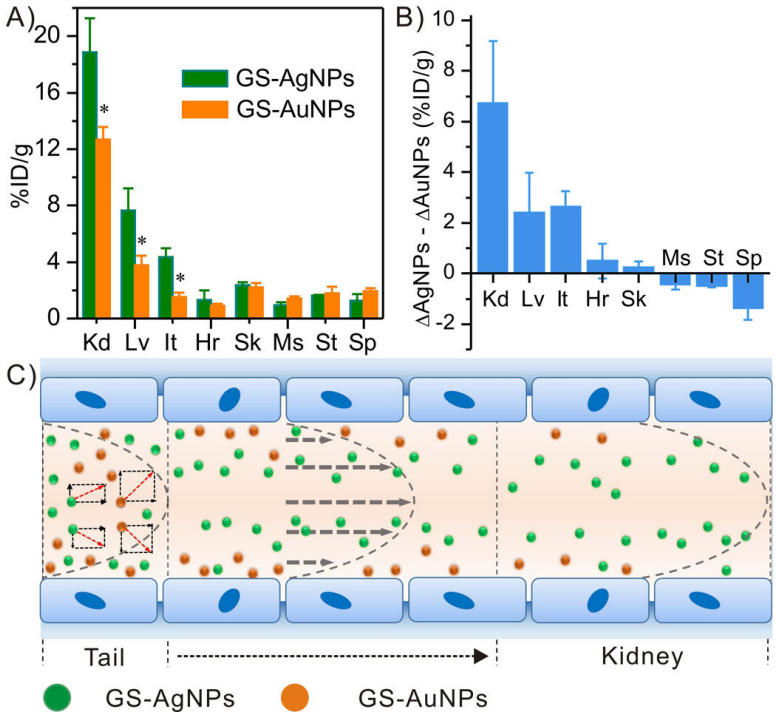

Figure 4.

The biodistribution study of GS-AuNPs and GS-AgNPs. A) 7-min biodistribution of GS-AgNPs and GS-AuNPs in major organs. B) The differences in the clearance of GS-AuNPs (ΔGS-AuNPs) and clearance of GS-AgNPs (ΔGS-AgNPs) in various organs at 7 min and 48 h p.i.. (Kd: kidney, It: intestine, Lv: liver, Hr: heart, Sk: skin, Ms: muscle, St: stomach, Sp: spleen; %ID/g=percentage of the injected dose per gram of tissues). *$p<0.005$. C) A hypothesized scheme showing the margination of GS-AuNPs (yellow) and GS-AgNPs (green) circulating in the blood stream after tail injection. Due to density-dependent margination, GS-AgNPs reach the kidneys faster than GS-AuNPs.